ACS APPLIED MATERIALS & INTERFACES

Research Article

www.acsami.org

Tin Dioxide@Carbon Core–Shell Nanoarchitectures Anchored on Wrinkled Graphene for Ultrafast and Stable Lithium Storage

Xunfu Zhou,[†] Weijian Liu,[†] Xiaoyuan Yu,[†] Yingju Liu,[†] Yueping Fang,*[,†] Steven Klankowski,[‡] Yiqun Yang,[‡] James Emery Brown,[‡] and Jun Li*[,‡]

[†]The Institute of Biomaterial, College of Science, South China Agricultural University, Guangzhou, Guangdong 510642, China

[‡]Department of Chemistry, Kansas State University, Manhattan, Kansas 66506, United States

Supporting Information

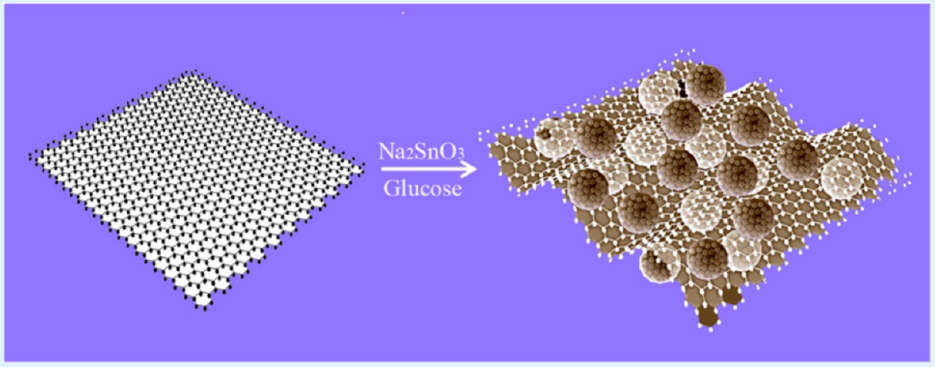

ABSTRACT: The SnO_2@C@GS composites as a new type of 3D nanoarchitecture have been successfully synthesized by a facile hydrothermal process followed by a sintering strategy. Such a 3D nanoarchitecture is made up of SnO_2@C core–shell nanospheres and nanochains anchored on wrinkled graphene sheets (GSs). Transmission electron microscopy shows that these core–shell nanoparticles consist of 3–9 nm diameter secondary SnO_2 nanoparticles embedded in about 50 nm diameter primary carbon nanospheres. Large quantities of core–shell nanoparticles are uniformly attached to the surface of wrinkled graphene nanosheets, with a portion of them further connected into nanochains. This new 3D nanoarchitecture consists of two different kinds of carbon-buffering matrixes, i.e., the carbon layer produced by glucose carbonization and the added GS template, leading to enhanced lithium storage properties. The lithium-cycling properties of the SnO_2@C@GS composite have been evaluated by galvanostatic discharge–charge cycling and electrochemical impedance spectroscopy. Results show that the SnO_2@C@GS composite has discharge capacities of 883.5, 845.7, and 830.5 mA h g^{-1} in the 20th, 50th and 100th cycles, respectively, at a current density of 200 mA g^{-1} and delivers a desirable discharge capacity of 645.2 mA h g^{-1} at a rate of 1680 mA g^{-1}. This new 3D nanoarchitecture exhibits a high capability and excellent cycling and rate performance, holding great potential as a high-rate and stable anode material for lithium storage.

KEYWORDS: *tin dioxide, graphene, anode, nanosheets, 3D nanoarchitecture, lithium-ion batteries*

1. INTRODUCTION

Rechargeable lithium-ion batteries (LIBs) have been widely applied in portable electronics, implantable medical devices, and power tools, and have increasing usage in hybrid or full electric vehicles.[1,2] Extensive efforts have been devoted to the development of new electrode materials with large reversible capacity, long cycle life, sound rate performance, and high safety standards.[3−8] At the same time, much attention has been focused on the improved conductivity of electrodes.[9−11]

SnO_2 is one of the most promising anode candidates, owing to its abundance, low discharge potential (<1.5 V), and high theoretical capacity (790 mA h g^{-1}).[12,13] However, the extremely high volume expansion (up to 250%) induced by the alloying reaction with lithium is the bottleneck for the practical application of SnO_2 anodes. The so-called pulverization problem can cause a breakdown in electrical contact between SnO_2 and the current collector, leading to quick capacity fading upon extended cycling.[14]

One of the mitigating strategies is to build unique nanostructured SnO_2 that can buffer the excessive volume change, which includes 0D nanoparticles,[15] 1D nanorods/nanowires/nanotubes,[16−18] 2D nanosheets,[19,20] and 3D hollow or porous nanostructures.[21,22] Some of these nanostructures exhibited enhanced reversible capacities in LIBs. Nevertheless, the improvement in the cyclability of such SnO_2-based anode materials is limited because the large specific volume change and the aggregation problem of nanoparticles in repetitive charging and discharging of the battery were not solved, which

Received: February 10, 2014
Accepted: April 30, 2014
Published: April 30, 2014

   dx.doi.org/10.1021/am5007194 | ACS Appl. Mater. Interfaces 2014, 6, 7434−7443

cause mechanical failure and the loss of electrical contact at the anode. Another effective approach is to introduce carbonaceous materials to form SnO_2/C composites,[23,24] including amorphous carbon, carbon nanotubes, and graphene.[25−29] Study of the SnO_2/C composites has well demonstrated that the elastic nature of carbon supports can provide a cushion effect against the volume strain. At the same time, carbon-based materials act as conductive paths that could promote electron transfer during the lithiation and delithiation process. However, while the SnO_2/amorphous carbon composites (especially for SnO_2@carbon core−shell nanostructures)[28,30−33] exhibit an excellent electrochemical cycling performance, the obtainable power density is rather poor because of the low electronic conductivity. Graphene sheet (GS), a honeycomb network of sp^2 carbon atoms, has attracted enormous interest as an intriguing substrate to build nanohybrids for energy storage applications.[34] GS has outstanding electrical conductivity, excellent mechanical flexibility, a high specific surface area of over 2600 $m^2\ g^{-1}$, and high thermal and chemical stability.[35−38] Various graphene-based SnO_2 hybrids have been developed and have shown improved lithium storage.[39−42] However, because the volume expansion ratios of graphene and tin during lithium insertion/deinsertion are dramatically different, the SnO_2 nanoparticles can peel off from the graphene surface during lithiation/delithiation, which led to the capacity fading in previous reports on SnO_2/graphene anodes.[41,42] Therefore, SnO_2/amorphous carbon/graphene would be an optimal choice to improve the power density and capacity stability of a SnO_2 electrode.[43,44] However, these reports[28,33] on SnO_2/amorphous carbon/graphene focused on amorphous carbon-coated SnO_2/graphene composites, which showed a lack of effective control of carbon layers on SnO_2, leading to incomplete carbon coating for these SnO_2/C composites. In addition, our previous studies[23,24] have demonstrated that the moderate thickness of the carbon shell for SnO_2@C composites contributes to optimal electrochemical performances for desirable lithium storage capacity and long cycle life.

In the present investigation, we report a new type of 3D nanoarchitecture, SnO_2@C core−shell nanospheres and nanochains anchored on wrinkled graphene sheets (SnO_2@C@GS), prepared by a novel and facile hydrothermal and sintering continuous approach. The similar approach can be used to synthesize SnO_2/graphene sheets (SnO_2/GS) composites, carbon@graphene sheets (C@GS) composites, and SnO_2 nanoparticles, respectively, as well as can be demonstrated in the preparation of SnO_2@C core−shell nanochains.[23,24] More importantly, the 3D nanoarchitecture of the SnO_2@C@GS composites, which integrates all of the aforementioned design principles, has several advantages as anode materials for LIBs, including large surface area, excellent mechanical flexibility, structural stability, and electrical conductivity. As a result, the obtained SnO_2@C@GS composites displayed superior electrochemical performance with large reversible capacity, excellent cycling lifetime, and high rate performance. They are particularly promising as anodes for ultrafast and stable lithium storage.

2. EXPERIMENTAL SECTION

2.1. Material Synthesis. Graphene oxide (GO) was first synthesized using a modified version of Hummers' method.[33] According to our previous works, the SnO_2@C@GS precursor was prepared by a facile hydrothermal process.[23,24] In a typical synthesis, 36 mg of GO was dispersed into 36 mL of deionized water by sonication for 1 h. Next, 284 mg of Na_2SnO_3 and 5 g of D-glucose were dissolved in the resultant GO solution by stirring for 0.5 h. The resultant mixture was then transferred into a 50 mL Teflon-lined stainless steel autoclave, sealed, and kept at 180 °C for 4 h in an oven before cooling to room temperature. The product was harvested by centrifugation and washed with deionized water and ethanol. Under the same conditions and different reactants via the same hydrothermal process (Table.1), the above approach was used to prepare a SnO_2/GS precursor in the absence of glucose, single SnO_2 nanoparticles in the absence of GO and glucose, and a C@GS precursor in the absence of Na_2SnO_3. Finally, the as-prepared SnO_2/GS, SnO_2@C@GS, and C@GS precursors are sintered at high temperature (700 °C) for 2 h under an argon atmosphere.[23,45]

Table 1. Reactant Comparison of the Precursors of the Samples Obtained after the Hydrothermal Process under the Same Conditions

precursor of the sample	reactants
SnO_2@C@GS	GO (36 mg), Na_2SnO_3 (284 mg), glucose (5 g), and H_2O (36 mL)
SnO_2@C[20,21]	Na_2SnO_3 (324 mg), glucose (6 g), and H_2O (40 mL)
SnO_2/GS	GO (36 mg), Na_2SnO_3 (284 mg), and H_2O (36 mL)
SnO_2	Na_2SnO_3 (284 mg) and H_2O (36 mL)
C@GS	GO (36 mg), glucose (5 g), and H_2O (36 mL)

2.2. Material Characterization. The structure and morphology of the as-prepared samples were analyzed by X-ray diffraction (XRD; Rigaku, D/max 2500v/pc), laser Raman spectroscopy (Renishaw in Via), field-emission scanning electron microscopy (FE-SEM; Philips FEI Quanta 200 FEG), and transmission electron microscopy (JEOL-2010 microscope operated at 200 kV). Nitrogen adsorption−desorption isotherms were measured on a Gemini-2360 analyzer (Micromeritics Co., USA) at 77 K. The Brunauer−Emmett−Teller (BET) method was utilized to calculate the specific surface area, while the Barrett−Joyner−Halenda method was used to derive pore-size distributions from the desorption branches of the isotherms. The total pore volumes, V_p, were estimated from the amount adsorbed at a relative pressure of P/P_0 = 0.95. In addition, thermogravimetric analysis (TGA) was carried out on a Netzsch TG 209 apparatus under an air flow at a rate of 50 mL min^{-1} with a heating rate of 10 °C min^{-1}.

2.3. Electrochemical Measurement. The electrochemical performance was tested by assembling CR2025 coin cells in a glovebox filled with ultrapure argon, using lithium metal as a counter anode. The working electrode was composed of active material (SnO_2@C/GS or SnO_2/GS, C/GS), carbon black (Super-P), and binder (PVDF) at a weight ratio of 80:10:10. A microporous polypropylene film (Celgard 2400) was elected as a separator, and a 1 M solution of $LiPF_6$ in ethylene carbonate and diethyl carbonate (1:1 by volume) was used as the electrolyte. The galvanostatic charge−discharge was conducted with a battery tester (Neware, Shenzhen, China). The profiles of charging and discharging curves were obtained over a voltage range of 5 mV to 2 V (vs Li^+/Li) at a current density of 200 mA g^{-1} after activation at lower current density. Electrochemical impedance spectroscopy measurements were performed in the frequency range from 100 kHz to 10 MHz by applying an alternating-current (ac) signal of 5 mV.

3. RESULTS AND DISCUSSION

The structure and composition of the as-prepared SnO_2@C@GS composites were initially investigated by XRD and Raman spectroscopy. The XRD pattern in Figure 1A provides clear evidence that the products are composed of one crystalline phase, namely, tetragonal SnO_2 with a cassiterite structure (JCPDS card no. 41-1445). No other phases were found. Calculated from the (110) peaks in the XRD pattern, the crystal size of the SnO_2 particles is about 5 nm. The

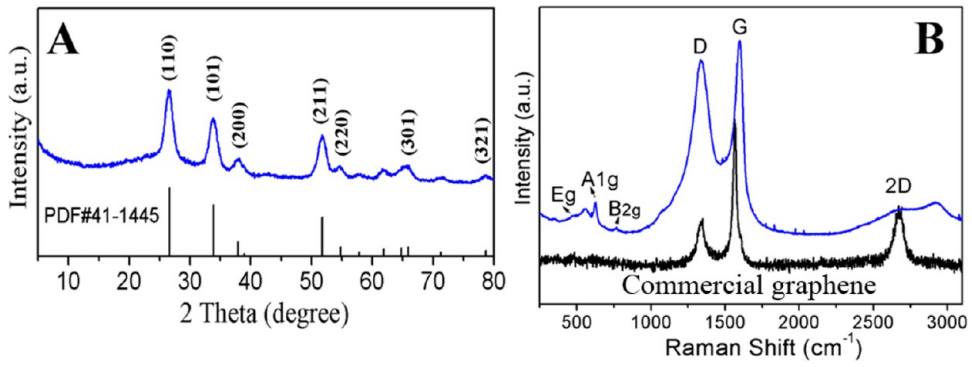

Figure 1. SnO_2@C@GS composites: (A) XRD pattern; (B) Raman spectra.

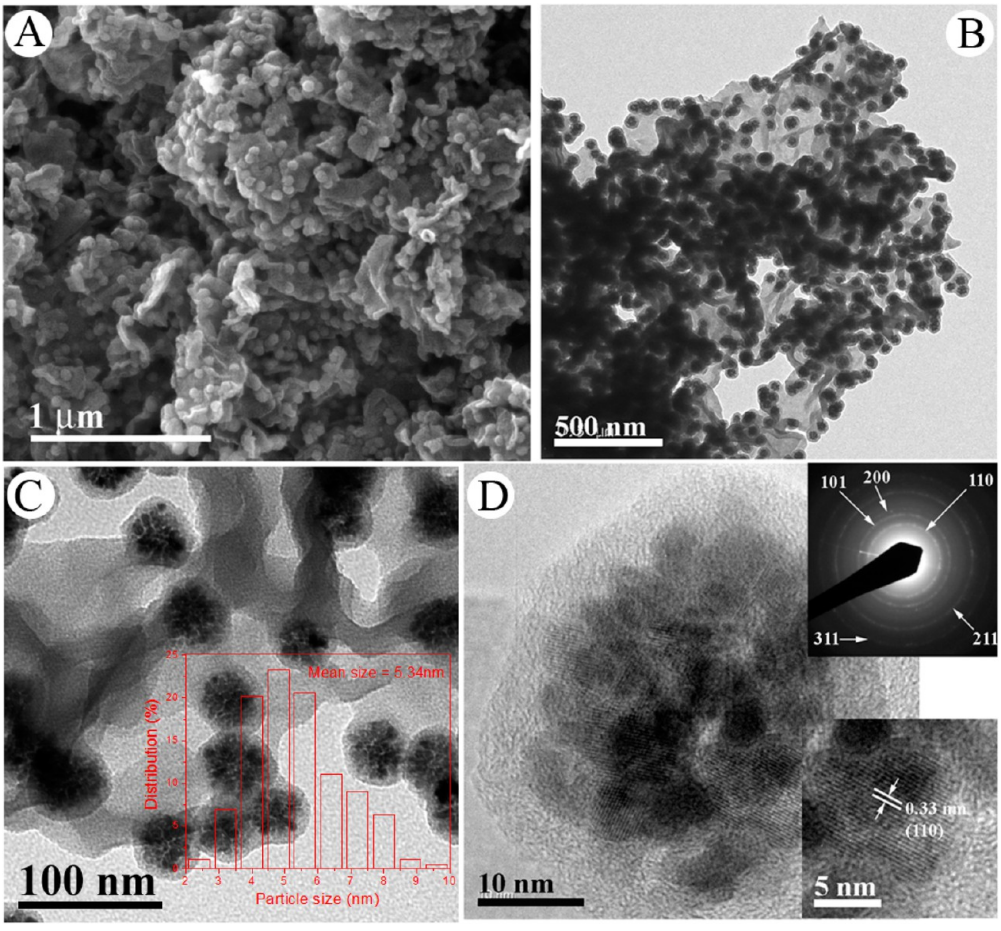

Figure 2. SnO_2@C@GS composites: (A) SEM; (B) typical TEM; (C) enlarged TEM; (D) HRTEM and enlarged HRTEM (inset, bottom) and the corresponding SAED pattern (inset, top).

unobservable peak at 10.3° shows that the reduction of GO to graphene is almost completed (Figure S1 in the Supporting Information, SI). The Raman spectra of the products also demonstrate the existence of carbon, graphene, and SnO_2 nanoparticles in the products.[27] As shown in Figure 1B, two typical carbon peaks at about 1340 cm^{-1} (D band) and 1595 cm^{-1} (G band) are observed. Meanwhile, three peaks can be observed at 477, 631, and 769 cm^{-1}, corresponding to E_g, A_{1g}, and B_{2g} vibrations of the SnO_2 nanoparticles.[29] The intensity ratio of the D band to the G band, I_D/I_G, of SnO_2@C@GS is higher than that of GS. The obvious enhancement of the intensity ratio in the SnO_2@C@GS composites can be attributed to the carbon coating and the increase of disorder in the graphene resulting from an aggressive hydrothermal reaction and the SnO_2 nanoparticles.[29]

The morphology and microstructure of the as-prepared SnO_2@C@GS composites were initially observed by FE-SEM and TEM. As shown by the SEM image (Figure 2A), it can be seen that a number of irregular nanosheets stack together and some particles coat on their surface. A larger-magnification SEM image shows that these irregular nanosheets are wrinkled and some particles (nanospheres) attach on their surface (Figure S2 in the SI). The TEM image (Figure 2B) shows that numerous core−shell nanospheres with a mean size of about 50 nm are attached on the surface of wrinkled nanosheet and some of them interconnect together to form a nanochain structure.

dx.doi.org/10.1021/am5007194 | ACS Appl. Mater. Interfaces 2014, 6, 7434−7443

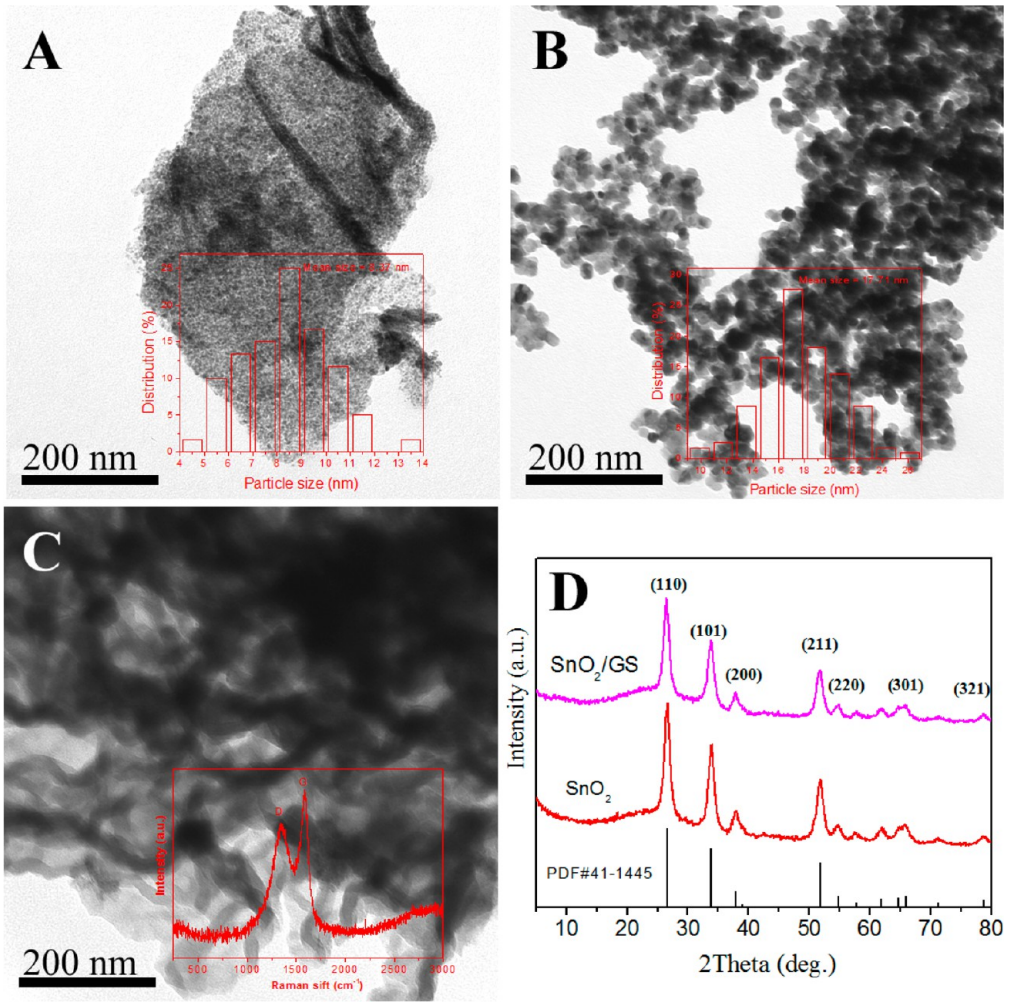

Figure 3. TEM images of SnO_2/GS (A), SnO_2 (B), and C@GS (C). XRD patterns (D) of SnO_2/GS and SnO_2. Particle size distributions of the SnO_2/GS composite (inset in A) and pure SnO_2 (inset in B). Raman spectrum of C@GS (inset in C).

The local magnification (Figure 2C) reveals more clearly that a lot of nanoparticles with a mean size of about 5.34 nm (inset in Figure 2C) gather and contact together within thin outer shells[23] to form inner cores with a diameter of 35 ± 5 nm, and these inner cores as well as graphene nanosheets are interconnected by the functional outer shells. A high-resolution TEM (HRTEM) image (Figure 2D) clearly shows a single core−shell nanosphere with a thickness of the carbon shell of about 5 nm and a diameter of the SnO_2 nanoparticles from 3 to 9 nm. The HRTEM image (inset in Figure 2D) shows clear lattice fringes for the (110) plane in tetragonal SnO_2 with a *d* spacing of 0.33 nm. The selected-area electron diffraction (SAED) pattern (inset in Figure 2D) can be indexed to tetragonal SnO_2. Obviously, the newly designed 3D nanoarchitectures of SnO_2@C@GS composites are made of SnO_2@carbon core−shell nanospheres and nanochains grown on wrinkled graphene nanosheets by a simple hydrothermal treatment and a subsequent sintering strategy.

In order to get insight into the growth mechanism of the 3D nanoarchitecture of SnO_2@C@GS composites, we carried out a group of control experiments using different reactants in the preparation of SnO_2/GS composites, single SnO_2 nanoparticles, and graphene@C composites, as shown in Figure 3. Control experiments were carried out by alternating different reactants (Table 1) under the same conditions via the same hydrothermal process. The SnO_2/GS composites (Figure 3A) show that very dense nanoparticles with diameters ranging between 4 and 14 nm (8−9 nm on average; inset in Figure 3A) are attached on the surface of a wrinkled sheet. The SnO_2 nanoparticles (Figure 3B) have diameters ranging between 10 and 26 nm (16−18 nm on average; inset in Figure 3B). However, the C@GS composites (Figure 3C) present the morphology of a soft, wrinkled, and curly film, which is only composed of carbon materials identified by Raman spectroscopy (inset in Figure 3C). Upon comparison with that of GO (Figure S1 in the SI), it is very obvious that the C@GS composites are made from GO sheets coated with thin amorphous carbon layers. Figure 3D shows the XRD patterns of SnO_2/GS composites and SnO_2 nanoparticles, indicating the presence of SnO_2. To compare the size of SnO_2 nanoparticles in SnO_2@C@GS, SnO_2/GS composites, and pure SnO_2 nanoparticles, respectively, it is very clear that the diameters of SnO_2 nanoparticles of SnO_2@C@GS composites are the smallest, suggesting that glucose molecules can act as a surfactant to control the growth of SnO_2 nanoparticles. The overall synthetic procedure along with a detailed mechanism of SnO_2@C@GS composites is illustrated in Scheme 1. The SnO_2@C@GS composites as a new type of 3D nanoarchitecture have been successfully synthesized by a facile hydrothermal process (I) and a subsequent sintering treatment

dx.doi.org/10.1021/am5007194 | ACS Appl. Mater. Interfaces 2014, 6, 7434−7443

Scheme 1. Formation Process of a 3D Nanoarchitecture of SnO_2@C@GS Composites: (A) Graphite Oxide; (B) SnO_2@C@GS Precursor; (C) SnO_2@C@GS Composite; (D) Cross Section of SnO_2@C@GS composite; (E) SnO_2 Clusters, GO, and Glucose and (F) Hydrochar C@GS and Small Hydrochar C@SnO_2 Precursors

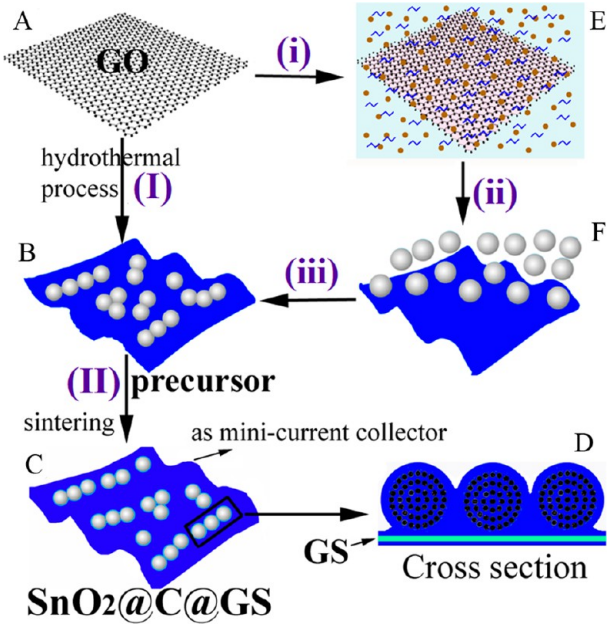

(II). At the beginning of the hydrothermal process, GO (A) should be further dispersed in an aqueous solution of glucose, and Na_2SnO_3 hydrolyzes to form a lot of small SnO_2 clusters (E). Because of weak interaction such as van der Waals forces, hydrogen bonding, or electrostatic repulsion, which is often vulnerable to strong extraneous elements,[46,47] glucose molecules are adsorbed onto the surface of GOs as well as SnO_2 clusters similarly to surfactant molecules (i). With an increase of the temperature, the glucose carbonizes hydrothermally to form a hydrochar layer on the surface of GOs (hydrochar C@GS precursor) and SnO_2 clusters (small hydrochar C@SnO_2 nanoparticles), respectively (F). Small hydrochar C@SnO_2 nanoparticles further aggregate to form a core–shell nanosphere or nanochain structure (ii). A 3D nanoarchitecture of the SnO_2@C@GS precursor (B) is formed by further cross-linking hydrochar layers of the nanospheres or nanochain and hydrochar C@GS precursor (iii). Finally, the SnO_2@C@GS precursor is heated at high temperature (700 °C) for 2 h under an argon atmosphere, and a SnO_2@C@GS composite (C) is achieved. Scheme 1D shows the cross section of the SnO_2@C@GS composite, suggesting that GS and SnO_2 nanoparticles are coated by the same amorphous carbon layer. Thus, the entire carbon layer including sandwiched GS can be used as a mini current collector.

The total carbon content (the GS and carbon resulting from carbonization of glucose) of the SnO_2@C/GS composites was determined by TGA (Figure 4A). The results show that no weight loss is observed for the SnO_2 nanoparticles (black line). However, an abrupt mass loss occurs between 350 and 550 °C, indicating the oxidation and decomposition of amorphous carbon and graphene in air. The mass fraction of graphene in the SnO_2/GS sample is about 6 wt % (red line), and the mass fraction of SnO_2 in the SnO_2@C@GS sample can be easily determined to be about 47 wt % (blue line), suggesting that the total amounts of graphene and amorphous carbon in SnO_2@C/GS may be around 53 wt %.

The surface area of the SnO_2@C/GS composite was characterized by nitrogen adsorption and desorption isotherms (Figure 4B). The surface area of the SnO_2@C/GS composites is 354.59 m^2 g^{-1}. In addition, the average pore diameter is about 5.08 nm, including two main pore sizes distributed in 2.5 nm (derived from hydrothermal carbon) and 70 nm (derived from wrinkled GSs and SnO_2@C core–shell nanospheres).[48,49] The pore volume is 0.45 cm^3 g^{-1}, which provides a large number of open channels as passages of the electrolyte and improves the diffusion rate of lithium ions during the cycling processes.

The discharge–charge curves for the 1st, 2nd, 5th, 20th, and 50th cycles of the electrodes made with single SnO_2 nanoparticles (Figure 5A) and SnO_2/GS (Figure 5B), SnO_2@C@GS (Figure 5C), and C@GS (Figure 5D) carried out in the voltage range of 5 mV to 2.0 V (vs Li) at a current density of 200 mA g^{-1} after activation at a lower current density. As shown in Figure 5A,B, the voltage plateau at 0.8–1.2 V is observed for the first two samples at the first discharge step, which stands for a conversion reaction between SnO_2 and Li^+, leading to the formation of Sn and Li_2O.[50] The following long

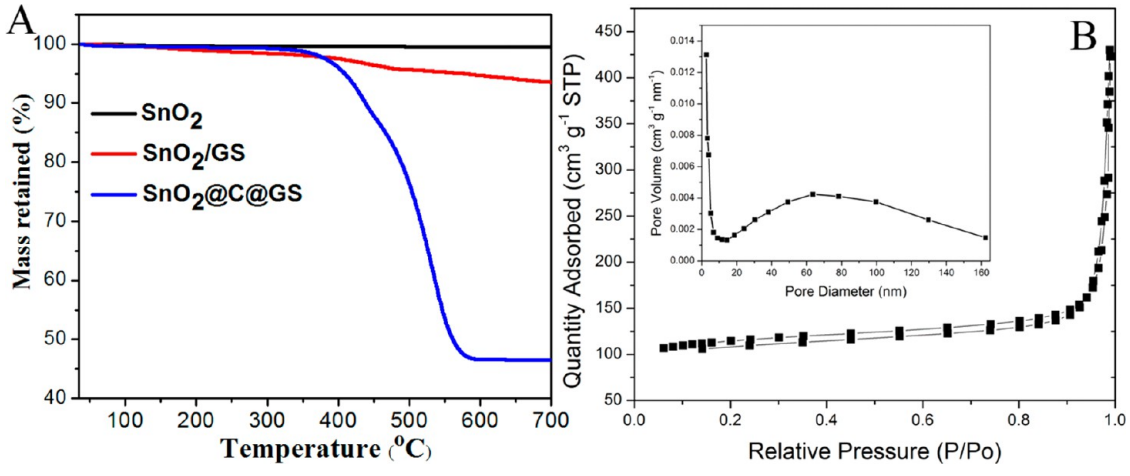

Figure 4. (A) TGA curves of the SnO_2@C@GS, SnO_2/GS, and SnO_2 samples. (B) Nitrogen adsorption–desorption isotherm curves and pore-size distributions of the SnO_2@C@GS composite.

dx.doi.org/10.1021/am5007194 | ACS Appl. Mater. Interfaces 2014, 6, 7434–7443

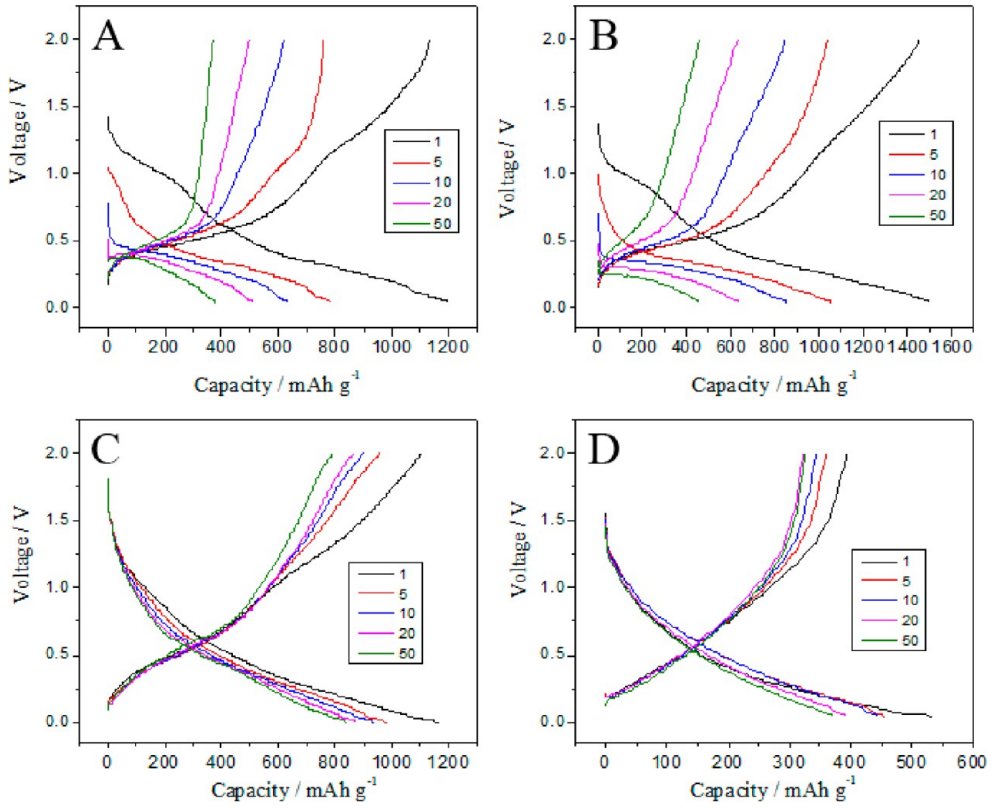

Figure 5. Charge and discharge curves of SnO_2 nanoparticles (A) and SnO_2/GS (B), SnO_2@C/GS (C), and C@GS (D) composites obtained at the 1st, 5th, 10th, 20th, and 50th cycles.

slope profiles of the SnO_2@C@GS composites indicated the formation of Li−Sn alloys and Li^+ intercalation into amorphous carbon and graphene. Because the major Li_2O is formed in the first cycle, the plateau at 0.8−1.2 V almost disappears at the second cycle. Compared with the single SnO_2 nanoparticles and SnO_2/GS, no remarkable change in the charge−discharge profile of SnO_2@C@GS composites was observed after 50 cycles (Figure 5C), indicating a stable cycling performance due to the controlled volume expansion and pulverization of well-dispersed nanosized SnO_2. However, for the C@GS composite (Figure 5D), it possesses a very low discharge capacity of 535 mA h g^{-1}, which is much lower than that of the first three samples, indicating a high first discharge capacity of SnO_2@C@GS composites mainly from well-dispersed SnO_2 nanoparticles.

The cycling performance of SnO_2 nanoparticles and single SnO_2/GS and SnO_2@C@GS composites at a current density of 200 mA g^{-1} with a voltage range of 5 mV to 2.0 V over 100 cycles is presented in Figure 6. The first specific discharge capacity of SnO_2 nanoparticles and SnO_2/GS and SnO_2@C@GS composites reach 1215.8, 1501.5, and 1164.6 mA h g^{-1}, respectively. All three samples have a large and irreversible capacity, which is due to the formation of an amorphous Li_2O matrix and intense surface reactions with the Li−Sn compounds as well as the electrolyte solution.[45] With an increasing number of cycles, the Coulombic efficiency of the SnO_2@C@GS composite becomes almost 100% from the 20th to 100th cycle, and SnO_2@C@GS composites have discharge capacities of 883.5, 845.7, and 830.5 mA h g^{-1} in the 20th, 50th, and 100th cycles, respectively. However, the capacities of the single SnO_2 are 538.3, 369.3, and 258.6 mA h g^{-1} in the 20th, 50th and 100th cycles, respectively. Also, the capacities of SnO_2/GS are 640.6, 466.6, and 322.9 mA h g^{-1} in the 20th, 50th, and 100th cycles, respectively. To our knowledge, the main reason for a rapid fading of the SnO_2/GS electrode, which leads to pulverization of the electrode, is a large volume expansion of SnO_2 that occurs during the charge−discharge cycle.[49,51,52] Therefore, SnO_2/GS results in very low capacity retention and only reaches a reversible capacity of 337.5 mA h g^{-1} in the 100th cycle. Moreover, in order to investigate the higher rate performance of SnO_2@C/GS, we have implemented the charge and discharge testing at 3360 mA g^{-1} for 100 cycles, with the result presented in Figure S3 (see the SI). It can be seen that the specific discharge capacity is 754.2 and 421.6 mA h g^{-1} at the 1st and 100th cycles, respectively. This value is higher than the theoretical capacity of graphite (370 mA h g^{-1}), indicating that the cyclability of the SnO_2@C/GS electrode is desirable for lithium storage practical applications.

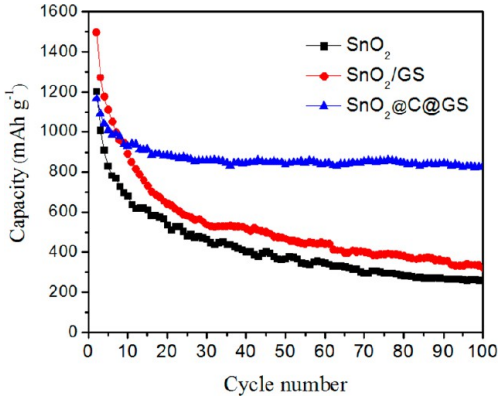

Figure 6. Cycling performance of the SnO_2 nanoparticles and SnO_2/GS and SnO_2@C@G composites at a current density of 200 mA g^{-1}.

dx.doi.org/10.1021/am5007194 | ACS Appl. Mater. Interfaces 2014, 6, 7434−7443

As shown in Figure 7, the rate performances of the as-obtained single SnO_2 nanoparticles and SnO_2/GS and SnO_2@C@GS samples are also studied. The SnO_2@C@GS composite displays excellent rate capability and delivers reversible capacities of 950.3, 843.3, 781.8, 721.7, and 645.2 mA h g^{-1} at high current densities of 105, 210, 420, 840, and 1680 mA g^{-1}, respectively. In addition, after the current rate returns to 105 mA g^{-1}, the electrode delivers a specific discharge capacity of about 889.4 mA h g^{-1}. Upon an increase in the discharge rates to 105, 210, 420, 840, and 1680 mA g^{-1}, the reversible capacities of single SnO_2 are maintained at 706.0, 520.4, 363.3, 256.4, and 144.9 mA h g^{-1}, respectively. The reversible capacities of SnO_2/GS are 834.0, 708.7, 583.5, 404.5, and 219.6 mA h g^{-1} with increasing discharge rates to 105, 210, 420, 840, and 1680 mA g^{-1}. Obviously, this result indicates that the SnO_2@C@GS nanocomposites are able to endure a variety of different current densities and have a perfect capacity recovery performance, which is a desirable characteristic for high-power LIB applications.

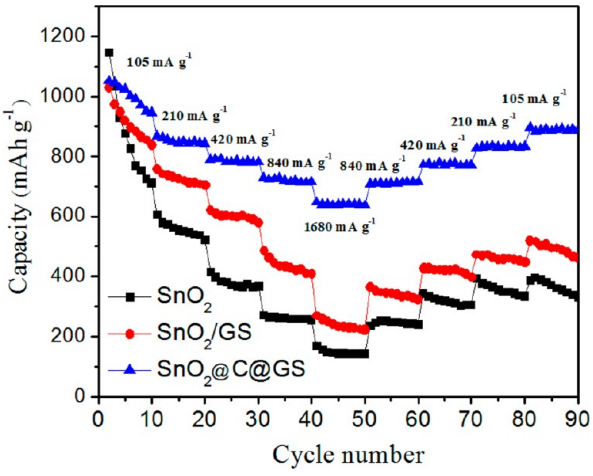

Figure 7. Rate performances of the SnO_2@C@GS composite and SnO_2/GS and SnO_2 nanoparticles without the first cycle.

The ac impedance data of single SnO_2, SnO_2/GS, and SnO_2@C@GS composites after cycling were measured. Figure 8 shows that the diameter of the semicircle for the single SnO_2 electrode in the high-to-medium-frequency region is biggest in the three materials. Also, the diameter of the semicircle for SnO_2/GS is bigger than SnO_2@C@GS composites, suggesting that the internal resistance of SnO_2/GS is greater than that of the SnO_2@C@GS composite. On the basis of the above results, the carbon shells and GS can improve the conductivity of the composites, which consequently enhances the electrochemical performance of SnO_2@C@GS composites.

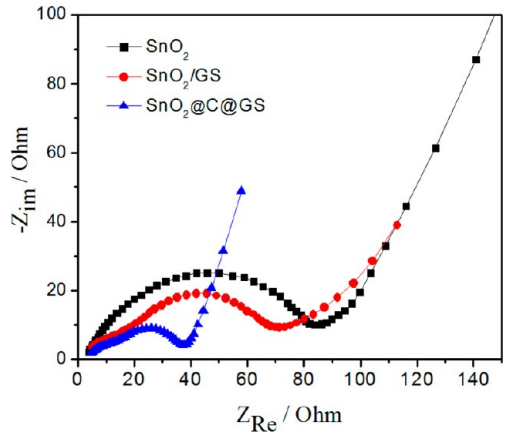

Figure 8. ac impedance data of SnO_2 nanoparticles and SnO_2/GS and SnO_2@C@GS composites after cycling.

Most importantly, the structural morphology changes before and after cycling performance testing was studied to understand the high capacity and good cyclability of the SnO_2@C@GS electrode. Figure 9 displays the SEM and TEM images of SnO_2@C@GS before and after charge−discharge cycling at 3360 mA g^{-1} for 100 cycles. As can be seen, some changes in the morphology and nanostructure of SnO_2@C@GS occurred. Especially, the SnO_2 particles no longer show clear nanocluster structures because of the repeated lithium alloying and dealloying. However, energy-dispersive X-ray (EDX) spectrometry measurement (Figure S4 in the SI) affirms that SnO_2@C@GS after charge−discharge cycling at 3360 mA g^{-1} for 100 cycles contains carbon, tin, and oxygen with Sn:O:C ≈ 1.78:37.63:60.59 atomic ratio, whereas excess oxygen may come from the oxidation of lithium. It can be estimated that there are still about 20 wt % of SnO_2 residues in the nanostructure of SnO_2@C@GS. It is obvious that critical evidence for the improved electrochemical performance of SnO_2@C@GS has been confirmed because of the physical buffer function of carbon shells to prevent the large volume change of SnO_2 anodes.

It is well-known that the electrochemical performance is closely related to the material nanostructures. Evidently, the cycling and rate performances of the SnO_2@C@GS composites are better than those of the SnO_2/GS, SnO_2@C, and SnO_2/C/graphene composites reported previously.[28,33,40−45] Expressly, compared with SnO_2@C nanochains,[23,24] the discharge capacity has been greatly improved from about 300 mA h g^{-1} of SnO_2@C nanochains to 645.2 mA h g^{-1} of SnO_2@C@GS at a high rate of 1680 mA g^{-1}. There is no doubt about that the cycling and rate performances of SnO_2-based electrodes have been greatly improved herein by the rational integration of small SnO_2 nanoparticles, amorphous carbon, and GS.

By all accounts, there are several reasons facilitating the high performances of the present 3D nanoarchitecture of SnO_2@C@GS composites as anode materials for LIBs: (i) The small SnO_2 nanoparticles allow for good accommodation of the large volume changes and readily relax the stress that occurs in bulk or micrometer-sized materials. Also, this small nanostructure provides a very high electrochemically active area, which results in an improved lithium storage capacity. (ii) Uniform thin carbon layers coated on SnO_2 and graphene have the ability to resist the large strain that occurs during the lithiation process and therefore succeeds in circumventing the pulverization issue. (iii) 2D carbon nanostructures of SnO_2@C@GS themselves could store lithium and act as a mini current collector. This mini-current collector could promote electron transfer during the lithiation and delithiation process, which has been proven by the ac impedance data above. (iv) 3D superstructures made up of close-packed SnO_2@C@GS with a porous configuration (BET surface area = 354.59 m^2 g^{-1} and total pore volume = 0.45 m^3 g^{-1}) provide a large number of open channels as passages of the electrolyte and improve the diffusion rate of lithium ions during the cycling processes.

Apart from the above-mentioned four reasons, an important source of high capacity, good cycling, and rate performance

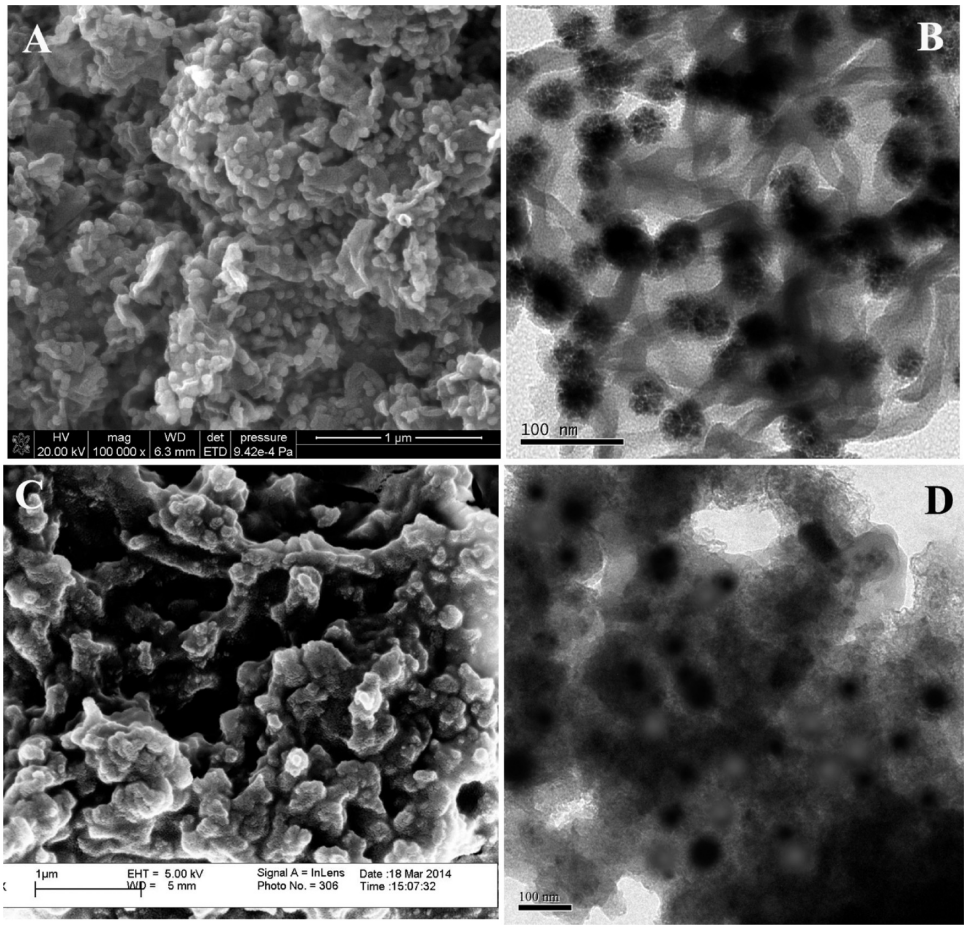

Figure 9. SEM and TEM images of SnO_2@C@GS before (A and B) and after (C and D) charge−discharge cycling at 3360 mA g^{-1} for 100 cycles.

should be the synergy arising from the ultrafine SnO_2 particles embedded in the carbon nanoshells and the interface interaction with graphene in the composites. As a result of synergistic effects arising from the ultrafine SnO_2 active particles, uniform carbon coating, and a steady graphene skeleton, the SnO_2@C@GS electrodes exhibit consistently higher capacities than SnO_2@C[23,24] and SnO_2/GS electrodes.[27,28]

4. CONCLUSION

The SnO_2@C@GS composites as a new type of 3D nanoarchitecture have been successfully synthesized by an easy hydrothermal and sintering continuous process. This 3D nanoarchitecture is made up of uniformly distributed SnO_2@C core−shell nanoparticle chains anchored on wrinkled GSs. The SnO_2@C@GS composites show significantly improved cycle lives and rate performance compared with the electrodes consisting of SnO_2/GS and SnO_2@C nanochains because of the active function of the graphene nanosheets in the composites and ultrafine SnO_2 particles hidden in the center of the carbon spheres. The SnO_2@C@GS composites delivered 645.2 mA h g^{-1} at a rate of 1680 mA g^{-1}, which showed a desirable rate performance of this composite electrode. The successful synthesis of the composite materials by the hydrothermal treatment of GO and $NaSnO_3$ in aqueous solutions of glucose can be an effective way of preventing graphene restacking and SnO_2 nanoparticle agglomeration. We believe that the highly conductive carbon layer and sandwiched GSs act as effective multiscale current collectors that can dramatically improve electron transport of the SnO_2 electrode and stabilize the power output of LIBs.

■ ASSOCIATED CONTENT

Ⓢ Supporting Information

Supplementary figures. This material is available free of charge via the Internet at http://pubs.acs.org.

■ AUTHOR INFORMATION

Corresponding Authors

*Phone: 8620-85285565. Fax: 8620-85285565. E-mail: ypfang@scau.edu.cn.

*Phone: 785-532-0955. Fax: 785-532-6666. E-mail: junli@ksu.edu.

Notes

The authors declare no competing financial interest.

■ ACKNOWLEDGMENTS

This research was supported by the NSF of China (Grants 20963002, 21173088, and 21105030), the Key Academic Program of the Third Phase "211 Project" of South China Agricultural University.

■ REFERENCES

(1) Armand, M.; Tarascon, J. M. Building Better Batteries. *Nature* **2008**, *451*, 652−657.

(2) Chen, J. S.; Lou, X. W. SnO_2-Based Nanomaterials: Synthesis and Application in Lithium-Ion Batteries. *Small* **2013**, *9*, 1877−1893.
(3) Bhattacharyya, R.; Key, B.; Chen, H.; Best, A. S.; Hollenkamp, A. F.; Grey, C. P. In Situ NMR Observation of The Formation of Metallic Lithium Microstructures in Lithium Batteries. *Nat. Mater.* **2010**, *9*, 504−510.
(4) Luo, B.; Fang, Y.; Wang, B.; Zhou, J.; Song, H.; Zhi, L. Two Dimensional Graphene−SnS_2 Hybrids with Superior Rate Capability for Lithium Ion Storage. *Energy Environ. Sci.* **2012**, *5*, 5226−5230.
(5) Luo, B.; Wang, B.; Liang, M.; Ning, J.; Li, X.; Zhi, L. Reduced Graphene Oxide-Mediated Growth of Uniform Tin-Core/Carbon-Sheath Coaxial Nanocables with Enhanced Lithium Ion Storage Properties. *Adv. Mater.* **2012**, *24*, 1405−1409.
(6) Reddy, M. V.; Subba Rao, G. V.; Chowdari, B. V. R. Metal Oxides and Oxysalts as Anode Materials for Li Ion Batteries. *Chem. Rev.* **2013**, *113*, 5364−5457.
(7) Yang, S.; Feng, X.; Ivanovici, S.; Müllen, K. Fabrication of Graphene-Encapsulated Oxide Nanoparticles: Towards High-Performance Anode Materials for Lithium Storage. *Angew. Chem., Int. Ed.* **2010**, *49*, 8408−8411.
(8) Recham, N.; Chotard, J. N.; Dupont, L.; Delacourt, C.; Walker, W.; Armand, M.; Tarascon, J. M. A 3.6 V Lithium-Based Fluorosulphate Insertion Positive Electrode for Lithium-Ion Batteries. *Nat. Mater.* **2010**, *9*, 68−74.
(9) Xia, T.; Zhang, W.; Li, W. J.; Oyler, N. A.; Liu, G.; Chen, X. B. Hydrogenated Surface Disorder Enhances Lithium Ion Battery Performance. *Nano Energy* **2013**, *2*, 826−835.
(10) Xia, T.; Zhang, W.; Murowchick, J. B.; Liu, G.; Chen, X. B. A Facile Method to Improve the Photocatalytic and Lithium-Ion Rechargeable Battery Performance of TiO_2 Nanocrystals. *Adv. Energy Mater.* **2013**, *3*, 1516−1523.
(11) Xia, T.; Zhang, W.; Murowchick, J.; Liu, G.; Chen, X. B. Built-in Electric Field-Assisted Surface-Amorphized Nanocrystals for High-Rate Lithium-Ion Battery. *Nano Lett.* **2013**, *13*, 5289−5296.
(12) Deng, D.; Kim, M. G.; Lee, J. Y.; Cho, J. Green Energy Storage Materials: Nanostructured TiO_2 and Sn-Based Anodes for Lithium-Ion Batteries. *Energy Environ. Sci.* **2009**, *2*, 818−837.
(13) Huang, J. Y.; Zhong, L.; Wang, C. M.; Sullivan, J. P.; Xu, W.; Zhang, L. Q.; Mao, S. X.; Hudak, N. S.; Liu, X. H.; Subramanian, A.; Fan, H.; Qi, L.; Kushima, A.; Li, J. In Situ Observation of The Electrochemical Lithiation of a Single SnO_2 Nanowire Electrode. *Science* **2010**, *330*, 1515−1520.
(14) Wang, C.-M.; Xu, W.; Liu, J.; Zhang, J.-G.; Saraf, L. V.; Arey, B. W.; Choi, D.; Yang, Z.-G.; Xiao, J.; Thevuthasan, S.; Baer, D. R. In Situ Transmission Electron Microscopy Observation of Microstructure and Phase Evolution in a SnO_2 Nanowire During Lithium Intercalation. *Nano Lett.* **2011**, *11*, 1874−1880.
(15) Guo, Z. P.; Du, G. D.; Nuli, Y.; Hassan, M. F.; Liu, H. K. Ultra-Fine Porous SnO_2 Nanopowder Prepared via a Molten Salt Process: A Highly Efficient Anode Material for Lithium-Ion Batteries. *J. Mater. Chem.* **2009**, *19*, 3253−3257.
(16) Liu, J.; Li, Y.; Huang, X.; Ding, R.; Hu, Y.; Jiang, J.; Liao, L. Direct Growth of SnO_2 Nanorod Array Electrodes for Lithium-Ion Batteries. *J. Mater. Chem.* **2009**, *19*, 1859−1864.
(17) Meduri, P.; Pendyala, C.; Kumar, V.; Sumanasekera, G. U.; Sunkara, M. K. Hybrid Tin Oxide Nanowires as Stable and High Capacity Anodes for Li-Ion Batteries. *Nano Lett.* **2009**, *9*, 612−616.
(18) Ye, J.; Zhang, H.; Yang, R.; Li, X.; Qi, L. Morphology-Controlled Synthesis of SnO_2 Nanotubes by Using 1D Silica Mesostructures as Sacrificial Templates and Their Applications in Lithium-Ion Batteries. *Small* **2010**, *6*, 296−306.
(19) Ding, S.; Wen Lou, X. SnO_2 Nanosheet Hollow Spheres with Improved Lithium Storage Capabilities. *Nanoscale* **2011**, *3*, 3586−3588.
(20) Wang, C.; Zhou, Y.; Ge, M.; Xu, X.; Zhang, Z.; Jiang, J. Z. Large-Scale Synthesis of SnO_2 Nanosheets with High Lithium Storage Capacity. *J. Am. Chem. Soc.* **2009**, *132*, 46−47.
(21) Wang, Z.; Zhou, L.; Lou, X. W. Metal Oxide Hollow Nanostructures for Lithium-ion Batteries. *Adv. Mater.* **2012**, *24*, 1903−1911.
(22) Wu, H. B.; Chen, J. S.; Hng, H. H.; Wen Lou, X. Nanostructured Metal Oxide-Based Materials as Advanced Anodes for Lithium-Ion Batteries. *Nanoscale* **2012**, *4*, 2526−2542.
(23) Zhang, B.; Yu, X.; Ge, C.; Dong, X.; Fang, Y.; Li, Z.; Wang, H. Novel 3-D Superstructures Made up of SnO_2@C Core−Shell Nanochains for Energy Storage Applications. *Chem. Commun.* **2010**, *46*, 9188−9190.
(24) Yu, X.; Yang, S.; Zhang, B.; Shao, D.; Dong, X.; Fang, Y.; Li, Z.; Wang, H. Controlled Synthesis of SnO_2@Carbon Core−Shell Nanochains as High-Performance Anodes for Lithium-Ion Batteries. *J. Mater. Chem.* **2011**, *21*, 12295−12302.
(25) Huang, Y. S.; Wu, D. Q.; Han, S.; Li, S.; Xiao, L.; Zhang, F.; Feng, X. L. Assembly of Tin Oxide/Graphene Nanosheets into 3D Hierarchical Frameworks for High-Performance Lithium Storage. *ChemSusChem* **2013**, *6*, 1510−1515.
(26) He, M.; Yuan, L.; Hu, X.; Zhang, W.; Shu, J.; Huang, Y. A SnO_2@carbon Nanocluster Anode Material with Superior Cyclability and Rate Capability for Lithium-ion Batteries. *Nanoscale* **2013**, *5*, 3298−3305.
(27) Zhong, C.; Wang, J.; Chen, Z.; Liu, H. SnO_2−Graphene Composite Synthesized via an Ultrafast and Environmentally Friendly Microwave Autoclave Method and Its Use as a Superior Anode for Lithium-Ion Batteries. *J. Phys. Chem. C* **2011**, *115*, 25115−25120.
(28) Zhu, J.; Lei, D.; Zhang, G.; Li, Q.; Lu, B.; Wang, T. Carbon and Graphene Double Protection Strategy to Improve the SnO_x Electrode Performance Anodes for Lithium-Ion Batteries. *Nanoscale* **2013**, *5*, 5499−5505.
(29) Cheng, J.; Xin, H.; Zheng, H.; Wang, B. One-Pot Synthesis of Carbon Coated-SnO_2/Graphene-Sheet Nanocomposite with Highly Reversible Lithium Storage Capability. *J. Power Sources* **2013**, *232*, 152−158.
(30) Lou, X. W.; Chen, J. S.; Chen, P.; Archer, L. A. One-Pot Synthesis of Carbon-Coated SnO_2 Nanocolloids with Improved Reversible Lithium Storage Properties. *Chem. Mater.* **2009**, *21*, 2868−2874.
(31) Liu, J.; Li, W.; Manthiram, A. Dense Core−Shell Structured SnO_2/C Composites as High Performance Anodes for Lithium Ion Batteries. *Chem. Commun.* **2010**, *46*, 1437−1439.
(32) Kong, J.; Tan, H. R.; Tan, S. Y.; Li, F.; Wong, S. Y.; Li, X.; Lu, X. A Generic Approach for Preparing Core−Shell Carbon−Metal Oxide Nanofibers: Morphological Evolution and Its Mechanism. *Chem. Commun.* **2010**, *46*, 8773−8775.
(33) Su, Y.; Li, S.; Wu, D.; Zhang, F.; Liang, H.; Gao, P.; Cheng, C.; Feng, X. Two-Dimensional Carbon-Coated Graphene/Metal Oxide Hybrids for Enhanced Lithium Storage. *ACS Nano* **2012**, *6*, 8349−8356.
(34) Huang, X.; Qi, X.; Boey, F.; Zhang, H. Graphene-Based Composites. *Chem. Soc. Rev.* **2012**, *41*, 666−686.
(35) Novoselov, K. S.; Geim, A. K.; Morozov, S. V.; Jiang, D.; Zhang, Y.; Dubonos, S. V.; Grigorieva, I. V.; Firsov, A. A. Electric Field Effect in Atomically Thin Carbon Films. *Science* **2004**, *306*, 666−669.
(36) Lee, C.; Wei, X.; Kysar, J. W.; Hone, J. Measurement of the Elastic Properties and Intrinsic Strength of Monolayer Graphene. *Science* **2008**, *321*, 385−388.
(37) Fasolino, A.; Los, J. H.; Katsnelson, M. I. Intrinsic Ripples in Graphene. *Nat. Mater.* **2007**, *6*, 858−861.
(38) Balandin, A. A.; Ghosh, S.; Bao, W.; Calizo, I.; Teweldebrhan, D.; Miao, F.; Lau, C. N. Superior Thermal Conductivity of Single-Layer Graphene. *Nano Lett.* **2008**, *8*, 902−907.
(39) Paek, S.-M.; Yoo, E.; Honma, I. Enhanced Cyclic Performance and Lithium Storage Capacity of SnO_2/Graphene Nanoporous Electrodes with Three-Dimensionally Delaminated Flexible structure. *Nano Lett.* **2008**, *9*, 72−75.
(40) Wang, D.; Kou, R.; Choi, D.; Yang, Z.; Nie, Z.; Li, J.; Saraf, L. V.; Hu, D.; Zhang, J.; Graff, G. L.; Liu, J.; Pope, M. A.; Aksay, I. A. Ternary Self-Assembly of Ordered Metal Oxide−Graphene Nano-

composites for Electrochemical Energy Storage. *ACS Nano* **2010**, *4*, 1587−1595.
(41) Li, Y.; Lv, X.; Lu, J.; Li, J. Preparation of SnO_2-Nanocrystal/Graphene-Nanosheets Composites and Their Lithium Storage Ability. *J. Phys. Chem. C* **2010**, *114*, 21770−21774.
(42) Ding, S.; Luan, D.; Boey, F. Y. C.; Chen, J. S.; Lou, X. W. SnO_2 Nanosheets Grown on Graphene Sheets with Enhanced Lithium Storage Properties. *Chem. Commun.* **2011**, *47*, 7155−7157.
(43) Zhu, J.; Zhang, G. H.; Yu, X. Z.; Li, Q. H.; Lu, B. A.; Xu, Z. Graphene double protection strategy to improve the SnO_2 electrode performance anodes for lithium-ion batteries. *Nano Energy* **2014**, *3*, 80−87.
(44) Lian, P. C.; Wang, J. Y.; Cai, D. D.; Ding, L. X.; Jia, Q. M.; Wang, H. H. Porous SnO_2@C/graphene Nanocomposite with 3D Carbon Conductive Network as a Superior Anode Material for Lithium-ion Batteries. *Electrochim. Acta* **2014**, *116*, 103−110.
(45) Ren, Y.; Zhang, J.; Liu, Y.; Li, H.; Wei, H.; Li, B.; Wang, X. Synthesis and Superior Anode Performances of TiO_2−Carbon−rGO Composites in Lithium-Ion Batteries. *ACS Appl. Mater. Interfaces* **2012**, *4*, 4776−4780.
(46) Tang, Z. Y.; Kotov, N. A. One-Dimensional Assemblies of Nanoparticles: Preparation, Properties, and Promise. *Adv. Mater.* **2005**, *17*, 951−962.
(47) Li, Z.; Li, Q.; Fang, Y.; Wang, H.; Li, Y.; Wang, X. Unique Mesoporous Carbon Microsphere/1-D MnO_2-Built Composite Architecture and Their Enhanced Electrochemical Capacitance Performance. *J. Mater. Chem.* **2011**, *21*, 17185−17192.
(48) Sevilla, M.; Fuertes, A. B. Chemical and Structural Properties of Carbonaceous Products Obtained by Hydrothermal Carbonization of Saccharides. *Chem.—Eur. J.* **2009**, *15*, 4195−4203.
(49) Yang, S.; Zhang, B.; Ge, C.; Dong, X.; Liu, X.; Fang, Y.; Wang, H.; Li, Z. Close-Packed Mesoporous Carbon Polyhedrons Derived from Colloidal Carbon Microspheres for Electrochemical Energy Storage Applications. *RSC Adv.* **2012**, *2*, 10310−10315.
(50) Xu, C.; Sun, J.; Gao, L. Synthesis of Multiwalled Carbon Nanotubes That Are Both Filled and Coated by SnO_2 Nanoparticles and Their High Performance in Lithium-ion Batteries. *J. Phys. Chem. C* **2009**, *113*, 20509−20513.
(51) Zhang, W.-M.; Hu, J.-S.; Guo, Y.-G.; Zheng, S.-F.; Zhong, L.-S.; Song, W.-G.; Wan, L.-J. Tin-Nanoparticles Encapsulated in Elastic Hollow Carbon Spheres for High-Performance Anode Material in Lithium-Ion Batteries. *Adv. Mater.* **2008**, *20*, 1160−1165.
(52) Tang, Y.; Wu, D.; Chen, S.; Zhang, F.; Jia, J.; Feng, X. Highly Reversible and Ultra-fast Lithium Storage in Mesoporous Graphene-based TiO_2/SnO_2 Hybrid Nanosheets. *Energy Environ. Sci.* **2013**, *6*, 2447−2451.